First estimates of fumarolic SO_2 fluxes from Putana volcano, Chile, using an ultraviolet imaging camera

K. Stebel [a,*], A. Amigo [b], H. Thomas [c], A.J. Prata [c]

[a] Norwegian Institute for Air Research, Instituttveien 18, 2007 Kjeller, Norway
[b] SERNAGEOMIN, Merced 22, Santiago, Chile
[c] Nicarnica Aviation AS, Gunnar Randers vei 24, 2007 Kjeller, Norway

ABSTRACT

Putana is a stratovolcano in the central Andes volcanic zone in northern Chile on the border with Bolivia. Fumarolic activiy has been visible at its summit crater at 5890 m altitude from long distances since the early 1800s. However, due to its remote location neither detailed geological studies have been made nor gas fluxes have been monitored and therefore its evolution remains unknown. On November 28, 2012 an ultraviolet (UV) imaging camera was transported to Putana and for about 30 min images of the fumaroles were recorded at 12 Hz. These observations provide the first measurements of SO_2 fluxes from the fumarolic field of Putana and demonstrate the applicability of the UV camera to detect such emissions. The measurement series was used to assess whether the sampling rate of the data influences the estimate of the gas flux. The results suggest that measurements made at 10 s and 1 min intervals capture the inherent (turbulent) variability in both the plume/wind speed and SO_2 flux. Relatively high SO_2 fluxes varying between 0.3 kg s^{-1} and 1.4 kg s^{-1}, which translates to 26 t/day and 121 t/day assuming constant degassing throughout the day, were observed on November 28, 2012. Furthermore, we demonstrate how an optical flow algorithm can be integrated with the SO_2 retrieval to calculate SO_2 fluxes at pixel level. Average values of 0.64 kg s^{-1} ± 0.20 kg s^{-1} and 0.70 kg s^{-1} ± 0.53 kg s^{-1} were retrieved from a "classical" transect method and the "advanced" optical flow based retrieval, respectively. Assuming constant emissions throughout all times, these values would results in an average annual SO_2 burden of 20–22 kT.

1. Introduction

1.1. Background

The emission of sulfur dioxide (SO_2) to the atmosphere from volcanic sources has important environmental and geological implications. SO_2 impacts air quality and detrimentally affects plant health in the immediate vicinity of volcanoes (e.g., Delmelle et al., 2002; Hansell and Oppenheimer, 2004). Furthermore, fluctuations in sulfur dioxide can often provide insights into changes in magma storage and movement and may precede eruptive activity (e.g., Barberi et al., 1992). Knowledge of SO_2 fluxes at volcanoes elucidates information about the transfer of species such as CO_2 and halogens, as well as SO_2 itself, between major Earth reservoirs. This has significant implications for the global chemical cycles (Oppenheimer et al., 2011). Current estimates of the volcanic SO_2 budget are based on satellite measurements (e.g., Realmuto et al., 1994; Carn et al., 2003; Theys et al., 2013) and field campaigns (e.g., Andres and Kasgnoc, 1998, and references therein) which typically are restricted to actively degassing vents. The exact contribution from volcanoes is poorly constrained due to the logistical and technical difficulties arising in measuring emissions from passively degassing volcanoes, where concentrations are low, but may be sustained over a long period of time. Fumarolic emissions from volcanic fields are of importance when considering the global geochemical cycles; previous studies predominantly used in situ methods to measure trace element ratios (e.g., Shinohara et al., 2011; Zelenski et al., 2013). So far, because of the difficulties associated with measuring low gas fluxes, relatively few attempts have been made to constrain sulfur dioxide fluxes from fumaroles (e.g., Tamburello et al., 2011a; Padrón et al., 2012). This paper provides the first estimates of SO_2 emissions from an example of sustained, low concentration degassing at Putana volcano, Chile and demonstrates the applicability of an ultraviolet (UV) imaging camera to detect such emissions.

1.2. UV remote sensing

While imaging techniques to monitor SO_2 emissions from industrial stacks using an ultraviolet video system have been known for nearly

40 years (Exton, 1976), UV imaging cameras were used for the first time for SO_2 observations from volcanoes by Mori and Burton (2006) and Bluth et al. (2007) as a fast alternative to the widely used miniaturised USB-powered grating spectrometers (e.g., McGonigle et al., 2002; Galle et al., 2003; McGonigle, 2005; Horton et al., 2006; McGonigle, 2007; Kantzas et al., 2009). These spectrometers had successfully replaced the popular COrrelation SPECtrometer (COSPEC) instrument, the latter being used for three decades to monitor SO_2 fluxes from industrial stacks as well as from volcanoes (e.g., Moffat and Millan, 1971; Casadevall et al., 1983; Stoiber et al., 1983; Stix et al., 2008).

Nowadays, ultraviolet remote sensing is commonly used for monitoring of volcanic sulfur emissions (e.g., Oppenheimer, 2010) and mini-DOAS instruments are widely spread for automated monitoring of SO_2 fluxes, for example at Soufrière Hills Volcano, Montserrat (Edmonds et al., 2003), at Mt. Etna, Italy (Salerno et al., 2009), within the FLux Automatic Measurement (FLAME) network at Stromboli, Italy (Burton et al., 2009) and in particular through the global Network for Observation of Volcanic and Atmospheric Change (NOVAC) (Galle et al., 2010).

UV imaging cameras have quickly become a popular tool for ground-based remote sensing of volcanic emissions. The benefit of the technique was recognized when highly sensitive fast charge-coupled device (CCD) cameras became affordable. Initially the SO_2 cameras were equipped with a single filter in a spectral region where SO_2 is highly absorbing (~307 nm) (Bluth et al., 2007). The system (Mori and Burton, 2006) developed used a second band path filter centered around 330 nm to compensate for broad-band effects, e.g., light scattering by aerosols and condensed water droplets and aerosol (ash) absorption.

Since then, large improvements have been made with respect to instrumental development and monitoring strategies (Kantzas et al., 2010; Kern et al., 2010; Tamburello et al., 2011b), absolute calibration (Lübcke et al., 2013), the challenges related to radiative transfer and the influence of aerosols (Kern et al., 2013), and the determination of plume motion vectors for improved flux measurements (Peters et al., 2015). UV cameras have been used to monitor SO_2 emissions from volcanoes (typical fluxes ~ 10–100 kg s^{-1}; Burton et al., 2015, and references therein), power plants (~1–10 kg s^{-1}; McElhoe and Conner, 1986; Ajtai, 2012) and ships (~0.002–0.1 kg s^{-1}; Prata, 2014). So far, the only fumarole field observations using UV cameras were made by Tamburello et al. (2011a) at the La Fossa crater, Vulcano Island.

1.3. Putana volcano

Putana is a stratovolcano in the central Andes volcanic zone in northern Chile on the border with Bolivia (22°33′S, 67°51′W) with a peak altitude of 5890 m (González-Ferrán, 1995). The volcano summit crater of diameter 0.5 km consists of two inner craters, where fumarolic activity has been producing 100–500 m high plumes since the early 1800s (Tassi et al., 2011, and references therein), with the most recent eruption reported in early 19th century (Rudolph, 1955). Fumarolic activity remains significant with gas emission temperatures of 82–88 °C and source temperatures of 500 °C. In agreement with the relatively high temperatures found, the gas species are dominated by high SO_2 and H_2S concentrations (up to 53 mmol/mol and 8.5 mmol/mol, respectively) suggesting that magmatic degassing is the dominant fluid source (Tassi et al., 2011).

The volcano shows a well-preserved summit crater, satellite vents and several post-glacial lava flows. Despite the persistent degassing through high-temperature fumaroles, they form a weak satellite thermal anomaly reaching temperatures of only 5 K above the background (Jay et al., 2013). Deformation studies from InSAR indicated a period of uplift of 4 cm between September 2009 and January 2010 and coincident seismic swarms are indicative of magmatic movement beneath the surface (Henderson and Pritchard, 2013; Pritchard et al., 2014).

However, detailed geological studies have not been done and therefore its evolution remains unknown.

The aim of the paper is to provide first estimates of the SO_2 fluxes from the fumarolic field of Putana volcano and to demonstrate the applicability of a UV imaging camera to detect such emissions.

2. Hardware and methodology

2.1. SO_2 camera

The UV camera (frequently called SO_2 camera) is in this work based on an uncooled Hamamatsu C8484 UV camera with high quantum efficiency in the UV from 280 nm onward (>30% at 300 nm). The camera is fast sampling (12 Hz) and has a custom-made four-position filter-wheel equipped with two 10 nm wide filters centered at 310 nm and 325 nm, a UV broadband view and a blackened plate for automated dark-current measurement. The main specifications of this system, called Envicam-2, are given in Table 1.

For the measurements presented here a UV lens with a focal length of 25 nm (F/2.8 lens) was used. With a given CCD effective area of 6.25 mm × 4.76 mm the full field of view of the camera is therefore 14.3° × 10.9°. The camera is controlled from a laptop with a frame grabber via custom made software. Camera exposure times vary, depending on illumination conditions, between 12.4 s and 1 s. The system is equipped with a co-aligned miniature spectrometer (USB2000+ from Ocean Optics Inc.) and an integrated webcam to capture the general overview of the scene. The Envicam-2 imaging system is built into a protective casing, can be setup in about 10 min and can be powered either via mains power or a 12 V battery.

A precursor of this UV camera has recently been used to show that SO_2 cameras are, besides useful for monitoring volcanic and stack emissions, able to measure SO_2 fluxes from ships (Prata, 2014). A detailed overview of the instrumental parameters of the Envicam-2 is given in Kern et al. (2015), Table 1 where the authors present an intercomparison of seven state-of-the-art SO_2 cameras gathered during the first Plume Imaging Workshop at Mt. Stromboli, Italy, in June 2013.

2.2. Retrieval of SO_2 fluxes

The principles for the data analysis and calibration procedure for the UV camera are described in detail in Prata (2014), therefore only a short summary of the specifics applied to this dataset is given. Under optimum measurement conditions, i.e., negligible aerosol scattering, the SO_2 path concentration ρ [g m^{-2}], i.e., the concentration c integrated over the light-path L, can be estimated from the Beer–Bouguer–Lambert law as:

$$\rho = c \cdot L = \frac{1}{\sigma(\lambda)} \, ln \, \frac{I_o(\lambda)}{I(\lambda)} \tag{1}$$

with the SO_2 absorption cross section $\sigma(\lambda)$ at wavelength λ, the measured light intensity $I(\lambda)$ and the background light intensity $I_0(\lambda)$. The

Table 1
Main specifications of the Envicam-2.

Optics	25 mm UV lens F/2.8
Image size	1344 × 1024 pixels
Chip size	4.65 µm
Total field-of-view	14.3° × 10.9°
Filter 1	310 nm
Filter 2	325 nm
Filter 3	empty
Filter 4	dark
Sampling rate	12 Hz [35.7 Hz 4 × 4 binning]
Exposure setting	1 µs to 1 s
Detector	Hamamatsu C8484-16C
Digitization	12 bits

SO_2 absorption coefficient integrated over the passband of the filter is $\sigma = 2.343 \ e^{-19} \ cm^2$ molecule^{-1}, calculated from the laboratory data of Vandaele et al. (2009).

Background images can be modeled well using the same linear combination of a Gaussian and a cubic equation (see Prata, 2014, Eq. (5)). The digital number DN_o for a given image pixel p is approximated as:

$$DN_o(p) = A_0 exp\left(-\frac{x^2}{2}\right) + A_3 + A_4 p + A_5 p^2 + A_6 p^3$$
$$x(p) = \frac{p - A_1}{A_2}. \tag{2}$$

The fit parameters A_0–A_2 describe the height, center and width of the exponent. A_3–A_6 describe the constant, linear, quadratic and cubic terms, respectively.

The SO_2 path concentration can then be estimated from the ratio between the measured dark corrected digital signal of the fore- $(DN - DN_d)$ and background image $(DN_o - DN_{o,d})$ via a linear calibration with intercept $A = 0.27 \ m^2 \ g^{-1}$. An offset is fitted in the SO_2 free area of the SO_2 images to account for illumination differences between calibration and observations.
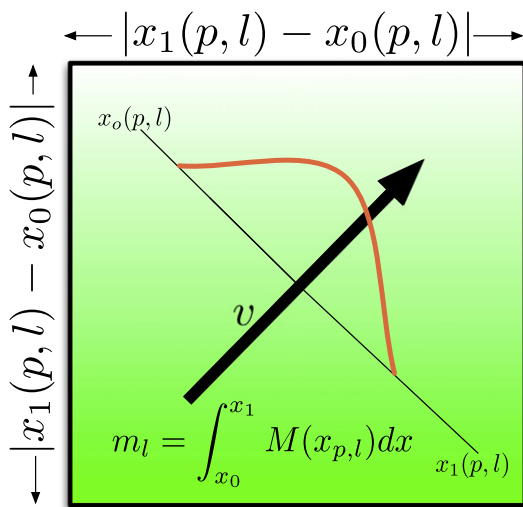
$$\rho_{SO_2} = A \ ln \frac{DN_o - DN_{o,d}}{DN - DN_d} + B. \tag{3}$$

From this the SO_2 flux s_e can be calculated as

$$s_e = w v_p \ \text{with} \ w = \int_{z_1}^{z_0} \rho_{SO_2}(z) dz \tag{4}$$

with the average plume speed v_p and the integrated SO_2 path concentration w. v_p has been retrieved from the displacement of features at the top of thermals in consecutive sets of difference images with time. w has been calculated along a transect line across the plume, orthogonal to the main plume dispersal direction.

An alternative algorithm has been developed to compute the SO_2 flux at (super-)pixel level from the UV camera images. The methodology is illustrated in Fig. 1 and the reader is referred to Lopez et al. (2015) for further details. The algorithm allows the computation of the SO_2 flux at pixel-row, p and line, l locations within the plume. First, SO_2 mass loadings (M) are estimated from the UV camera retrieval. Second, the plume velocity vectors (v) using an optical flow retrieval are calculated. The optical flow algorithm follows that of Farnebäck (2003), two, using a polynomial expansion method to approximate the neighborhood of each pixel with a quadratic polynomial. Integration of M along the line x_0 to x_1 that is orthogonal to the velocity vector, passing through the center of the super-pixel group, determines the SO_2 mass per unit length (mL). Multiplying mL by the plume velocity gives the SO_2 flux at pixel-row p and line l. This value of the SO_2 flux is assigned to a square area, the size of a super-pixel.

3. Results

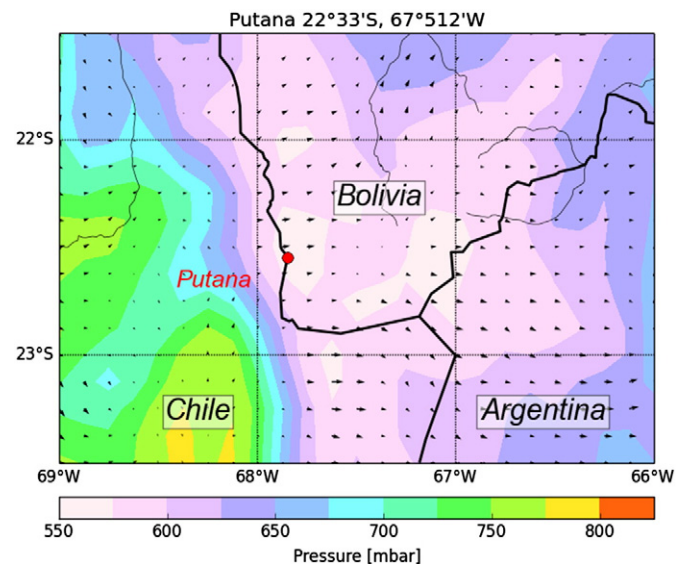### 3.1. Background and meteorological conditions

Fig. 2 shows the atmospheric surface pressure field (color-coded) with an overlay showing the 10 m wind vector fields from the European Centre for Medium-Range Weather Forecasts (ECMWF) analysis for the day of the UV camera measurements, November 28, 2012. At the location of Putana, atmospheric pressure values of 590 mbar, temperatures of 280 K and westerly winds with low speeds of 1.8 m s^{-1} are found.

Few aerosol observations are available for the central volcanic zone of the Andes. An indication for the aerosol loading can be found in the observations by Cordero et al. (2014). For January 15, 2013 the authors derived a total UV aerosol loading AOD = 0.15 and a single-scattering albedo SSA = 0.7 on the Chajnantor plateau (23°00′S, 67°45′W, 5100 m). This shows an influence from wind-blown dust on the otherwise pristine and clear high altitude atmosphere.

Annual composite SO_2 images from the Ozone Monitoring Instrument (OMI) were unable to detect any sulfur dioxide emissions from Putana above the background noise of the instrument.

3.2. UV imaging camera measurements

The UV imaging camera was transported to Putana volcano by a 4WD vehicle and mounted at an altitude of 4935 m a.s.l. at 22°35′S, 67°53′W, approximately at a horizontal distance of 6150 m south–west of the volcano (see Fig. 3). The summit of Putana volcano (22°33′S, 67°51′W, 5890 m a.s.l.) is seen at a viewing elevation angle

Fig. 1. Graphic showing the method for calculating the SO_2 flux at pixel-row, p and line, l based on a plume velocity vector (v) estimated from the optical flow algorithm and mass loading (M) estimated from the UV retrieval. An integral along the path x_o to x_1, orthogonal to the plume velocity is performed to determine the mass per unit length (m_l). Multiplying m_l by the plume velocity gives the SO_2 flux at p, l. This value of the SO_2 flux is assigned to an area of dimension $|x_1 - x_0| \times |x_1 - x_0|$ (for further details see Lopez et al., in press).

Fig. 2. ECMWF analysis of 10-m wind fields [m s^{-1}] and surface pressure [mbar] (color-coded) are shown for November 28, 2012 12:00 UTC (8:00 local time). The data have a spatial resolution of 0.25° × 0.25°. The location of Putana volcano (22°33′S, 67°51′W) is marked in red.
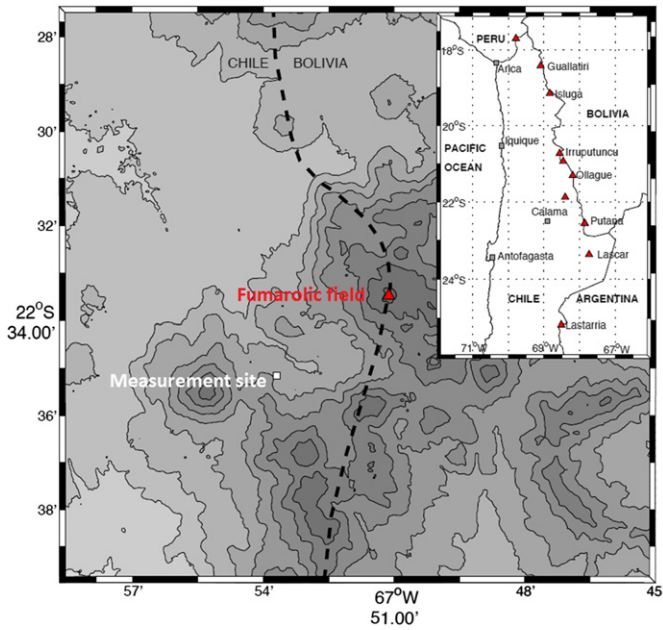
Fig. 3. Location map for Putana volcano. The fumarolic field (red triangle) lies inside the main vent along the Chilean–Bolivia border, and the measurement site (white square) is located circa 6 km south–west from the volcano summit. The gray scale indicates topographic altitude between 4400 and 5800 m a.s.l., getting darker every 200 m, taken from the ASTER-GDEM dataset. The inset shows volcanoes with passive degassing in the Central Andes of Chile. Main cities are named as well as the best known volcanoes.

of 8° above the horizontal. Power was supplied by a car battery and measurements were made over only a short period of time starting at 10:16 local time (LT) on November 28, 2012. Power availability and the difficult logistical conditions (high altitude and long drive) restricted the time period available for the measurements to just over 30 min.

Images were recorded at 12 Hz to capture the variability of the plume dynamics at high speed, using the on-band filter at 310 nm central wavelengths only. The observations were made under good light conditions, excellent visibility and a cloudless sky. Exposure times were about 0.03 s. A photo of the scene is given in Fig. 4 demonstrating the excellent visibility of the fumaroles at the volcano summit under the high altitude, cloud-free atmosphere.

Fig. 4. Photo of the solfatara (fumaroles) at the summit of Putana volcano taken on November 28, 2012.

An example raw image obtained during the field campaign at Putana volcano is shown in Fig. 5. The square pixel size of the CCD is $d_v = d_h = 1.13$ m, which corresponds to a full image dimension of about $D_h = 1500$ m horizontally and $D_v = 1150$ m vertically. The translucent fumaroles cover approximately one-third of the image. This is an optimal situation with respect to the estimation of the background image intensity from the plume-free area to both sides of the fumaroles. Due to the small field-of-view of the optics used to obtain the measurements the background is relative flat and can easily be estimated using the fitting procedure described above (see Eq. (2)). For calibration, custom made cylindrical quartz cells with 50 mm diameter to cover the entire field of view of the camera optics have been used. Fumarolic SO_2 fluxes are retrieved within the marked sub-region of the image (see white frame in Fig. 5).

3.3. SO_2 fluxes from the plume transect method

The "classical" method to calculate SO_2 flux, s_e is based on the estimation of an integrated SO_2 path concentration, w along a transect across the plume multiplied with the averaged plume speed, v_p vertical to this line. Plume speeds were derived from the spatial displacement of features at the upper edge of the fumaroles seen in consecutive difference image pairs. A transect line is drawn through the plume orthogonal to the direction of the wind vector (see black line in Fig. 6). Fig. 6 shows an SO_2 column density image of the Putana fumaroles at 10:30 LT on November 28, 2012. SO_2 path concentrations as high as 2.7 g m^{-2} are seen close to the vent. The gas stream mixes with the surrounding air and disperses quickly to values below 0.5 g m^{-2} about 70 m above the vent.

The rate of plume motion which can be resolved by the camera is limited by the pixel width and plume speed. Assuming a maximum plume (wind) speed of 10 m s^{-1} and a given pixel width of 1.13 m, the minimum time for motion between pixels is 0.113 s (8.85 Hz), which can be resolved within the data acquisition rate of the camera (12 Hz).

A set of short time series of plume speeds, integrated SO_2 column mass and SO_2 fluxes for three periods on the same day are shown in Fig. 7. The average plume speed v_p was 3.8 m s^{-1}, maximum values peaked at about 6 m s^{-1}. Sulfur dioxide fluxes varied between 0.3 kg s^{-1} and 1.4 kg s^{-1}, which translates to 26 t/day and 121 t/day assuming constant degassing.

Data from the camera were collected at 12 Hz sampling and averaged to 1 s values, over five short time periods of 0.5–1.5 min duration (see Table 2). This short period of measurements is used to assess whether the sampling rate of the data influences the estimate of the flux. It is expected that the flux may vary due to wind fluctuations as well as changes in the amount of sulfur dioxide from the fumaroles. Fig. 7 suggests that the wind speed is fairly constant: $v_p = 3.8 \pm 0.8$ m s^{-1} with a coefficient of variation (c_v) of ~0.21. The SO_2 mass loading is a little more variable. The mean and standard deviation of the mass per unit length are: $\mu = 178.9 \pm 49.7$ g m^{-1}, c_v ~ 0.28. The mean and standard deviation of the SO_2 flux for the whole dataset matches those for 10 s samples (~100 image frames), suggesting that measurements made both at 10 s or 1 min intervals capture the inherent (turbulent) variability in both the wind and SO_2 amount.

3.4. SO_2 fluxes from the optical flow algorithm

A more "advanced" algorithm for the estimation of SO_2 fluxes from UV camera images based on an optical flow algorithm was developed. The methodology is illustrated in Fig. 1 and described in more detail in Lopez et al. (2015). Whereas "classical" method only evaluates the observations along a given transect across the plume and average plume speeds orthogonal to the transect, the "advanced" retrieval allows the
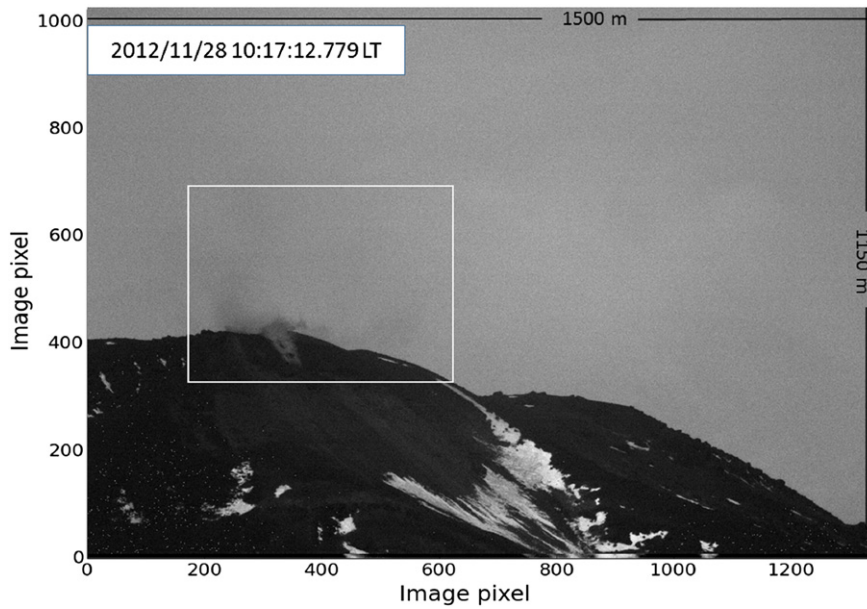
Fig. 5. Raw image of the Putana fumaroles at 10:17 LT on November 28, 2012. The box indicates the sub-region used for the analysis.

calculation of fluxes for individual pixels (here we use super-pixel regions of 20 × 20 pixels), as described above.

In Fig. 8 two images taken 36 s apart are shown. The snapshots illustrate variations in shape of the faint fumarole SO_2 plumes and plume velocity fields. The optical flow solution for the image sequence demonstrates the increasing wind speed with distance from the surface. The velocity field for the main fumarolic vent and even the movement within the faint structures circa 50 m below the main vent are well resolved.

Fig. 9 demonstrates how the optical flow algorithm can be integrated with the SO_2 retrieval to calculate fluxes for each super-pixel in the image. Mean sulfur fluxes of 0.9 ± 0.6 kg s^{-1} and 0.7 ± 0.6 kg s^{-1} were found for the two snapshots, which demonstrate the variability of the SO_2 fluxes within the fumarolic plume fields. In general, we see a good agreement between the optical flow based SO_2 fluxes rates with the values derived from the feature matching transect method. As expected the optical flow based retrieval shows larger variability as fluctuations over the whole plume geometry are taken into account.
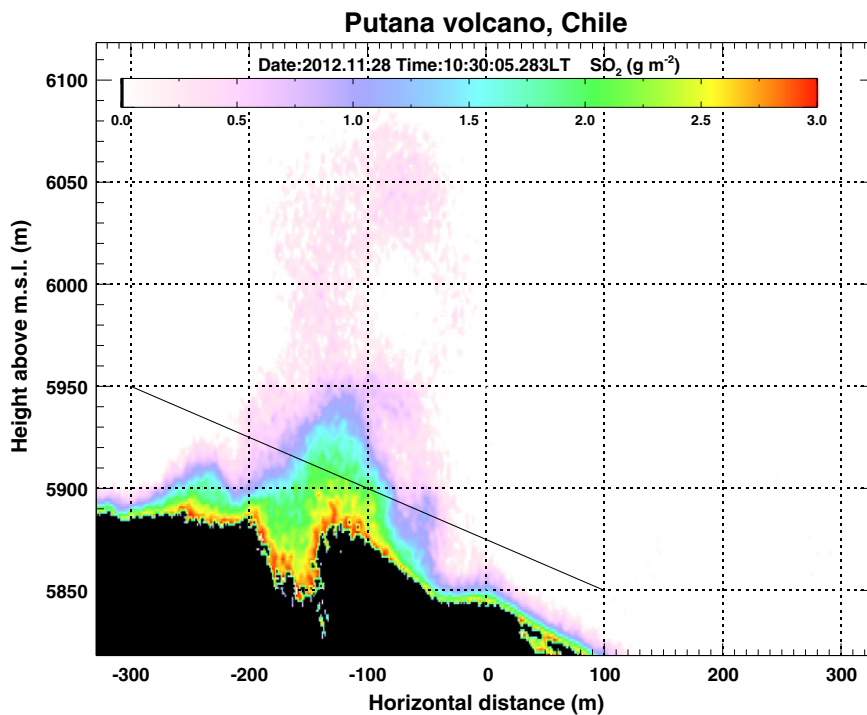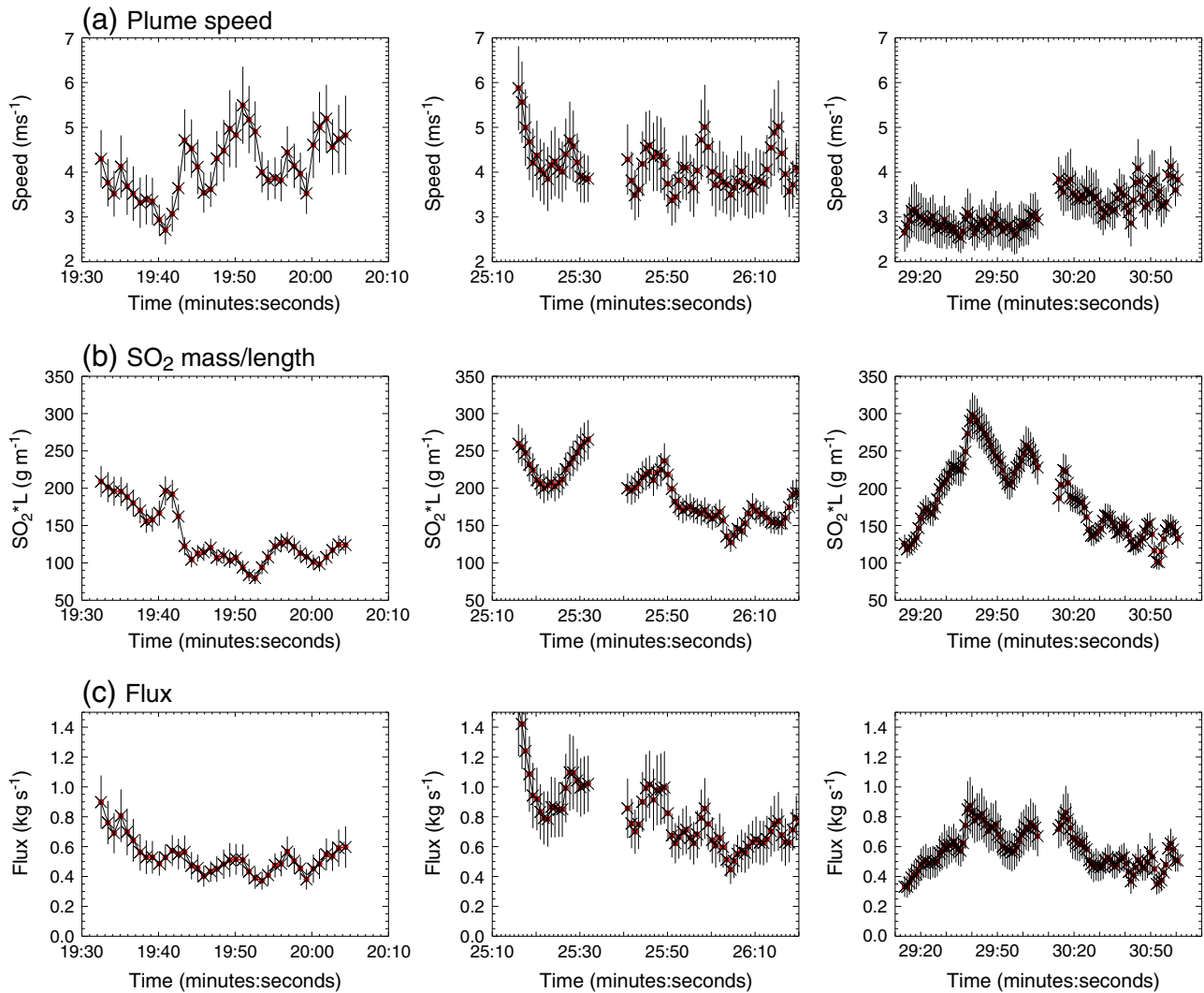

Fig. 6. SO_2 column density image of the Putana fumaroles at 10:30 LT on November 28, 2012. The straight line indicates the integral section used for the calculation of the integrated path concentration w.

Fig. 7. Estimates of plume speeds [m s⁻¹] (a: upper row panels), integrated SO₂ column mass [g m⁻¹] (b: middle row panels), and SO₂ flux [kg s⁻¹] (c: lower row panels) for three time periods on November 28, 2012. The times given are the minutes and seconds after 10 local time. Mean and averages values for 1 s intervals are shown.

3.5. Uncertainty discussion

For measurements of SO₂ emissions from ships using the same UV imaging camera type, (Prata, 2014) reported uncertainties on the order of 20% for the SO₂ flux and 15% for the SO₂ path-concentration under good light conditions. As a rough estimate we expect uncertainties in the same order of magnitude. Flux errors related to calibration errors and the image-background fitting procedure reported in Prata (2014) are

Table 2
Mean and standard deviation of the flux of SO₂ from the Putana fumaroles. Statistics have been calculated over different time ranges. The actual data were sampled at 0.1 s intervals and values are provided at 10 s intervals and an overall value for 3 min 20 s. A mean flux s_e of ~0.6 ± 0.2 kg s⁻¹ is found.

Period	s_e (kg s⁻¹)	$\pm \sigma$ (kg s⁻¹)
10 s	0.64	0.17
20 s	1.01	0.22
30 s	0.53	0.14
40 s	0.71	0.16
50 s	0.62	0.14
50 s	0.53	0.12
3 min 20 s	0.64	0.20

considered applicable for the observations made at Putana volcano. The camera location was estimated with GPS, but the absolute geometrical distance error is expected to be higher than the GPS uncertainty, because of the widespread nature of the fumarole field (50 m compared to 10 m given in Prata, 2014). The more "advanced" plume speed retrievals used here are estimated having lower uncertainties (estimated to 0.5 m s⁻¹ compared to 1 m s⁻¹). Light dilution effects depend on the absolute distance between camera and image, Rayleigh scattering and atmospheric background aerosol loading. The observations were done during clean atmospheric conditions at high altitudes, where the Rayleigh volume-scattering coefficient is reduced by a factor of about 0.6 compared to standard atmospheric conditions (volume scattering coefficient 0.125 km⁻¹ for pure air; Penndorf, 1957). Windblown dust cannot completely be disregarded, but for relatively low wind speeds its effect can be considered minimal. For a plume-source distance of about 6 km, the contrast attenuation can lead to a negative bias (~36% for 0.6 * Rayleigh atmosphere). The observations were performed with the on-band filter only. The second off-band-filter would be needed to compensate for broad-band effects, e.g., light scattering by aerosols and condensed water droplets and aerosol (ash) absorption. For optically thick and distant plumes radiative transfer related uncertainties for SO₂ column density measurement by UV camera can be very high or even inhibit sensible retrieval (for details see Kern et al., 2013). Typical biases of about 35%
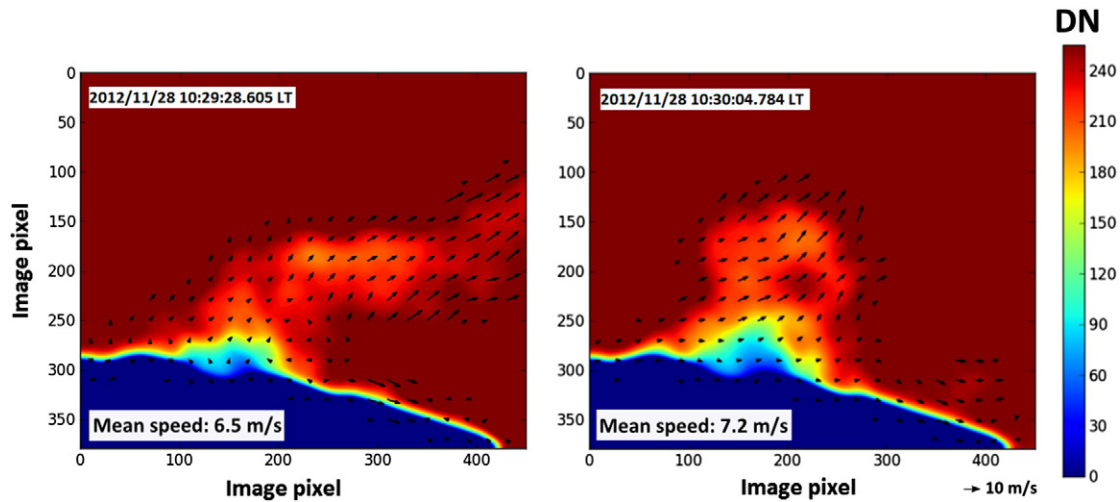
Fig. 8. Estimates of plume speeds [m s^{-1}] using an optical flow algorithm. Plume-speed vectors are overlain on top of the digital number *DN* for two images taken at 10:29:29 LT (left panel) and 10:30:05 LT (right panel).
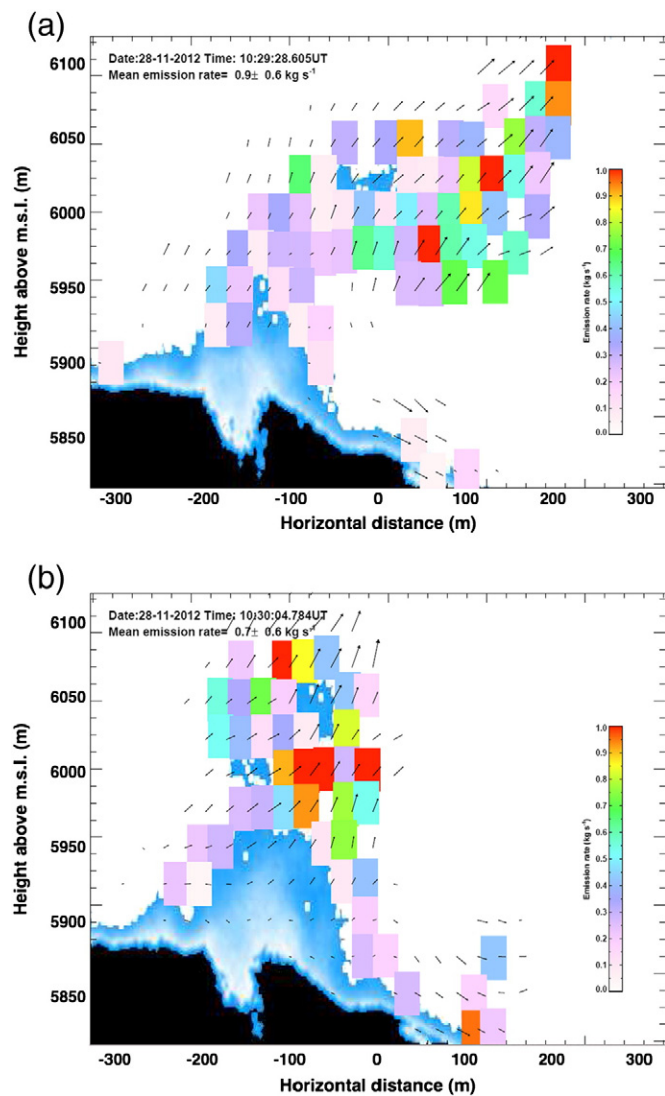

Fig. 9. SO$_2$ fluxes for the Putana fumarole field observed on November 28, 2012 at 10:29:29 LT (upper panel) and at 10:30:05 LT (lower panel). Mean fluxes are 0.9 ± 0.6 kg s^{-1} (at 10:29:29 LT) and 0.7 ± 0.6 kg s^{-1} (at 10:30:05 LT).

for moderate plume opacity are estimated by Kern et al. (2015, Fig. 1). For the very faint, basically ash free and translucent fumaroles of Putana volcano, we estimate a maximum of 10–15% bias by omitting the off-band observations. As some of the uncertainties may compensate each other (e.g., light dilutions leads to a low bias, while aerosol absorption results in a high bias), we estimate a total uncertainty of about 25–30%, which is comparable to the standard deviation of the SO$_2$ fluxes.

4. Discussion and conclusions

Activity at Putana volcano has been in a fumarolic state since the beginning of last century. Due to its remote location neither detailed geological studies have been made nor gas fluxes have been monitored and therefore its evolution remains unknown. Here we provide the first estimates of SO$_2$ fluxes from the fumarolic field of Putana from observations with an ultraviolet imaging camera made on November 28, 2012. The short time sequence recorded at 12 Hz demonstrates the applicability of the UV camera to detect such emissions.

For the area around Putana no local meteorological data were available. From the SO$_2$ camera observations, fairly constant, relatively low plume speeds were derived for the summit of Putana ($v_p = 3.8 \pm 0.8$ m s^{-1}). This is consistent with the general wind-field analysis from the ECMWF analysis showing low regional wind-speeds of circa 1.8 m s^{-1} (0.25 × 0.25 latitude/longitude grid). Nevertheless, the forecast wind speeds do not capture the plume velocity field well. The plume velocity field is a function of gas emissions, plume rise dynamics and the atmospheric background wind vector field. Only a fast imaging technique like the SO$_2$ camera used for the observations at Putana volcano, coupled with a motion detection algorithm, e.g. an optical flow retrieval, can capture its spatial distribution and rapid temporal variations.

The observations from November 28, 2012 show relatively high SO$_2$ fluxes varying between 0.3 kg s^{-1} and 1.4 kg s^{-1}. The short measurement series was used to assess whether the sampling rate of the data influences the estimate of the SO$_2$ flux. The flux mean and standard deviation of the whole data set matches those for 10 s samples (~100 image frames), suggesting that measurements made at 10 s and 1 min intervals capture the inherent (turbulent) variability in both the wind and SO$_2$ amount. If the 30 min observations are considered representative for observations throughout the day this would translate to daily SO$_2$ fluxes between 26 t/day and 121 t/day.

Furthermore, we demonstrate how an optical flow algorithm can be integrated with the SO$_2$ retrieval to calculate SO$_2$ fluxes at pixel

level. The optical flow solution demonstrates the increasing wind speed with distance from the surface. Even movement of faint structures outside of the main vent was resolved well. Mean estimates retrieved from the "classical" transect analysis and the "advanced" optical-flow based retrieval were comparable. Average SO_2 fluxes of 0.64 kg s^{-1} ± 0.20 kg s^{-1} and 0.70 kg s^{-1} ± 0.53 kg s^{-1} were derived from a "classical" transect method and the "advanced" optical flow based retrieval, respectively. As expected the optical flow based retrieval shows larger variability as fluctuations over the whole plume geometry are taken into account.

Assuming constant emissions throughout all times, these values would result in an average annual burden of 20–22 kT. It is known that magmatic degassing is the dominating fluid source for the Putana volcano, and fumarolic gas species are dominated by SO_2 and H_2S (Tassi et al., 2011), so the relatively high fluxes estimated here seem reasonable. A recently published study reported SO_2 fluxes for Putana of 0.46 kg s^{-1} for December 5, 2012, about a week after our field study, and 1.1 kg s^{-1} ± 0.9 kg s^{-1} for 3 days in December 2013 (Tamburello et al., 2014). These results are comparable with the observations reported here. Even higher SO_2 fluxes of 2.1 kg s^{-1} were seen during recent field observations at Putana using a portable mini-DOAS instruments (Bucarey, C., OVDAS-SERNAGEOMIN, pers. comm., May 2014).

The UV imaging camera observations presented here illustrate the need for additional studies and long-term monitoring of the fumarolic fields of Putana and other remote located volcanoes in the central Andes. With remote sensing equipment such as integrated camera-spectrometer systems generally becoming more automatized, a good estimate of the global sulfur budget could be gained in a cost-efficient way. Advanced image processing like optical flow based flux estimates derived from high frequency recordings can be considered as an important step forward. Such developments allow not only volcanic processes, but also turbulent variability in the gas emissions to be studied. Still, more work is needed to carefully exploit and inter-compare the different methods for plume-speed and flux retrievals from ultraviolet imaging cameras.

Acknowledgments

References

Ajtai, N., 2012. Optoelectronic techniques for atmospheric monitoring used for the assessment of natural hazard and techno-logical risk. (Ph.D. thesis). Babes-Bolyai University, Cluj-Napoca, Romania.

Andres, R.J., Kasgnoc, A.D., 1998. A time-averaged inventory of subaerial volcanic sulfur emissions. J. Geophys. Res. 103, 25251–25261. http://dx.doi.org/10.1029/98JD02091.

Barberi, F., Bertagnini, A., Landi, P., Principe, C., 1992. A review on phreatic eruptions and their precursors. J. Volcanol. Geotherm. Res. 52, 231–246. http://dx.doi.org/10.1016/0377-0273(92)90046-G.

Bluth, G., Shannon, J., Watson, I., Prata, A., Realmuto, V., 2007. Development of an ultraviolet digital camera for volcanic SO_2 imaging. J. Volcanol. Geotherm. Res. 161, 47–56. http://dx.doi.org/10.1016/j.jvolgeores.2006.11.004.

Burton, M., Caltabiano, T., Muré, F., Salerno, G., Randazzo, D., 2009. SO_2 flux from Stromboli during the 2007 eruption: results from the FLAME network and traverse measurements. J. Volcanol. Geotherm. Res. 182, 214–220. http://dx.doi.org/10.1016/j.jvolgeores.2008.11.025.

Burton, M., Prata, F., Platt, U., 2015. Volcanological applications of SO_2 cameras. J. Volcanol. Geotherm. Res. 300, 2–6.

Carn, S., Krueger, A., Bluth, G., Schaefer, S., Krotkov, N., Watson, I., Datta, S., 2003. Volcanic eruption detection by the Total Ozone Mapping Spectrometer (TOMS) instruments: a 22-year record of sulphur dioxide and ash emissions. Geol. Soc. Lond., Spec. Publ. 213, 177–202.

Casadevall, T., Rose, W., Gerlach, T., Greenland, L., Ewert, J., Wunderman, R., Symonds, R., 1983. Gas emissions and the eruptions of Mount St. Helens through 1982. Science 221, 1383–1385. http://dx.doi.org/10.1126/science.221.4618.1383.

Cordero, R.R., Seckmeyer, G., Damiani, A., Riechelmann, S., Rayas, J., Labbe, F., Laroze, D., 2014. The world's highest levels of surface UV. Photochem. Photobiol. Sci. 13, 70–81. http://dx.doi.org/10.1039/C3PP50221J.

Delmelle, P., Stix, J., Baxter, P., Garcia-Alvarez, J., Barquero, J., 2002. Atmospheric dispersion, environmental effects and potential health hazard associated with the low-altitude gas plume of Masaya volcano, Nicaragua. Bull. Volcanol. 64, 423–434. http://dx.doi.org/10.1007/s00445-002-0221-6.

Edmonds, M., Herd, R., Galle, B., Oppenheimer, C., 2003. Automated, high time-resolution measurements of SO_2 flux at Soufriére Hills Volcano, Montserrat. Bull. Volcanol. 65, 578–586. http://dx.doi.org/10.1007/s00445-003-0286-x.

Exton, R., 1976. Stack plume visualization system, US Patent 3931462. US National Aeronautics and Space Administration.

Farnebäck, G., 2003. Two-frame motion estimation based on polynomial expansion. Image Analysis. Springer, pp. 363–370.

Galle, B., Oppenheimer, C., Geyer, A., McGonigle, A., Edmonds, M., Horrocks, L., 2003. A miniaturised ultraviolet spectrometer for remote sensing of SO_2 fluxes: a new tool for volcano surveillance. J. Volcanol. Geotherm. Res. 119, 241–254. http://dx.doi.org/10.1016/S0377-0273(02)00356-6.

Galle, B., Johansson, M., Rivera, C., Zhang, Y., Kihlman, M., Kern, C., Lehmann, T., Platt, U., Arellano, S., Hidalgo, S., 2010. Network for Observation of Volcanic and Atmospheric Change (NOVAC) – A global network for volcanic gas monitoring: network layout and instrument description. J. Geophys. Res. 115. http://dx.doi.org/10.1029/2009JD011823.

González-Ferrán, O., 1995. Volcanes de Chile. Instituto Geográfico Militar, Santiago, Chile, p. 640.

Hansell, A., Oppenheimer, C., 2004. Health hazards from volcanic gases: a systematic literature review. Arch. Environ. Health 59, 628–639. http://dx.doi.org/10.1080/00039890409602947 (arXiv:http://dx.doi.org/10.1080/00039890409602947).

Henderson, S.T., Pritchard, M.E., 2013. Decadal volcanic deformation in the Central Andes Volcanic Zone revealed by InSAR time series. Geochem. Geophys. Geosyst. 14, 1358–1374. http://dx.doi.org/10.1002/ggge.20074.

Horton, K., Williams-Jones, G., Garbeil, H., Elias, T., Sutton, A., Mouginis-Mark, P., Porter, J., Clegg, S., 2006. Real-time measurement of volcanic SO_2 emissions: validation of a new UV correlation spectrometer (FLYSPEC). Bull. Volcanol. 68, 323–327. http://dx.doi.org/10.1007/s00445-005-0014-9.

Jay, J.A., Welch, M., Pritchard, M.E., Mares, P.J., Mnich, M.E., Melkonian, A.K., Aguilera, F., Naranjo, J.A., Sunagua, M., Clavero, J., 2013. Volcanic hotspots of the central and southern Andes as seen from space by ASTER and MODVOLC between the years 2000–2010. In: Pyle, D., Mather, T., Biggs, J. (Eds.), Remote sensing of volcanoes and volcanic processes: integrating observation and modelling. Geological Society of London, pp. 161–186.

Kantzas, E., McGonigle, A., Bryant, R., 2009. Comparison of low cost miniature spectrometers for volcanic SO_2 emission measurements. Sensors 9, 3256–3268. http://dx.doi.org/10.3390/s90503256.

Kantzas, E., McGonigle, A., Tamburello, G., Aiuppa, A., Bryant, R., 2010. Protocols for UV camera volcanic SO_2 measurements. J. Volcanol. Geotherm. Res. 194, 55–60. http://dx.doi.org/10.1016/j.jvolgeores.2010.05.003.

Kern, C., Kick, F., Lübcke, P., Vogel, L., Wöhrbach, M., Platt, U., 2010. Theoretical description of functionality, applications, and limitations of SO_2 cameras for the remote sensing of volcanic plumes. Atmos. Meas. Tech. 3, 733–749. http://dx.doi.org/10.5194/amt-3-733-2010.

Kern, C., Werner, C., Elias, T., Sutton, A.J., Lübcke, P., Kern, K., 2013. Applying UV cameras for SO_2 detection to distant or optically thick volcanic plumes. J. Volcanol. Geotherm. Res. 262, 80–89. http://dx.doi.org/10.1016/j.jvolgeores.2013.06.009.

Kern, K., Lübcke, P., Bobrowski, N., Campion, R., Mori, T., Smekens, J.F., Stebel, K., Tamburello, G., Burton, M., Platt, U., Prata, F., 2015. Intercomparison of SO_2 camera systems for imaging volcanic gas plumes. J. Volcanol. Geotherm. Res. 300, 22–36.

Lopez, T., Thomas, H., Prata, A., Amigo, A., Fee, D., Moriano, D., 2015. Volcanic plume characteristics determined using an infrared imaging camera. J. Volcanol. Geotherm. Res. 300, 148–166.

Lübcke, P., Bobrowski, N., Illing, S., Kern, C., Alvarez Nieves, J.M., Vogel, L., Zielcke, J., Delgado Granados, H., Platt, U., 2013. On the absolute calibration of SO_2 cameras. Atmos. Meas. Tech. 6, 677–696. http://dx.doi.org/10.5194/amt-6-677-2013.

McElhoe, H., Conner, W.D., 1986. Remote measurement of sulfur dioxide emissions using an ultraviolet light sensitive video system. J. Air Pollut. Control Assoc. 36, 42–47. http://dx.doi.org/10.1080/00022470.1986.10466043.

McGonigle, A., 2005. Volcano remote sensing with ground-based spectroscopy. Philos. Trans. R. Soc. A Math. Phys. Eng. Sci. 363, 2915–2929. http://dx.doi.org/10.1098/rsta.2005.1668.

McGonigle, A., 2007. Measurement of volcanic SO_2 fluxes with differential optical absorption spectroscopy. J. Volcanol. Geotherm. Res. 162, 111–122. http://dx.doi.org/10.1016/j.jvolgeores.2007.02.001.

McGonigle, A., Oppenheimer, C., Galle, B., Mather, T.A., Pyle, D., 2002. Walking traverse and scanning DOAS measurements of volcanic gas emission rates. Geophys. Res. Lett. 29. http://dx.doi.org/10.1029/2002GL015827 (46–1–46–4).

Moffat, A., Millan, M., 1971. The applications of optical correlation techniques to the remote sensing of SO_2 plumes using sky light. Atmos. Environ. 5, 677–690. http://dx.doi.org/10.1016/0004-6981(71)90125-9.

Mori, T., Burton, M., 2006. The SO_2 camera: a simple, fast and cheap method for ground-based imaging of SO_2 in volcanic plumes. Geophys. Res. Lett. 33 (L24804), 2006. http://dx.doi.org/10.1029/2006GL027916.

Oppenheimer, C., 2010. Ultraviolet sensing of volcanic sulfur emissions. Elements 6, 87–92. http://dx.doi.org/10.2113/gselements.6.2.87.

Oppenheimer, C., Scaillet, B., Martin, R., 2011. Sulfur degassing from volcanoes: source conditions, surveillance, plume chemistry and earth system impacts. Rev. Mineral. Geochem. 73, 363–421.

Padrón, E., Hernández, P., Pérez, N., Toulkeridis, T., Melián, G., Barrancos, J., Virgili, G., Sumino, H., Notsu, K., 2012. Fumarole/plume and diffuse CO_2 emission from Sierra Negra caldera, Galapagos archipelago. Bull. Volcanol. 74, 1509–1519. http://dx.doi.org/10.1007/s00445-012-0610-4.

Penndorf, R., 1957. Tables of the refractive index for standard air and the Rayleigh scattering coefficient for the spectral region between 0.2 and 20.0 μm and their application to atmospheric optics. J. Opt. Soc. Am. 47, 176–182.

Peters, N., Hoffmann, A., Barnie, T., Herzog, M., Oppenheimer, C., 2015. Use of motion estimation algorithms for improved flux measurements using SO_2 cameras. J. Volcanol. Geotherm. Res. 300, 58–69.

Prata, A.J., 2014. Measuring SO_2 ship emissions with an ultra-violet imaging camera. Atmos. Meas. Tech. 7, 1213–1229. http://dx.doi.org/10.5194/amt-7-1213-2014.

Pritchard, M.E., Henderson, S.T., Jay, J.A., Soler, V., Krzesni, D.A., Button, N.E., Welch, M.D., Semple, A.G., Glass, B., Sunagua, M., Minaya, E., Amigo, A., Clavero, J., 2014. Reconnaissance earthquake studies at nine volcanic areas of the central Andes with coincident satellite thermal and InSAR observations. J. Vol. Geotherm. Res. 280, 90–103. http://dx.doi.org/10.1016/j.jvolgeores.2014.05.004.

Realmuto, V.J., Abrams, M.J., Buongiorno, M.F., Pieri, D.C., 1994. The use of multispectral thermal infrared image data to estimate the sulfur dioxide flux from volcanoes: a case study from Mount Etna, Sicily, July 29, 1986. J. Geophys. Res. 99, 481–488. http://dx.doi.org/10.1029/93JB02062.

Rudolph, W., 1955. Lincancábur: mountain of the Atacameños. Geogr. Rev. XLV, 1–13.

Salerno, G., Burton, M., Oppenheimer, C., Caltabiano, T., Randazzo, D., Bruno, N., Longo, V., 2009. Three-years of SO_2 flux measurements of Mt. Etna using an automated UV scanner array: comparison with conventional traverses and uncertainties in flux retrieval. J. Volcanol. Geotherm. Res. 183, 76–83. http://dx.doi.org/10.1016/j.jvolgeores.2009.02.013.

Shinohara, H., Matsushima, N., Kazahaya, K., Ohwada, M., 2011. Magma-hydrothermal system interaction inferred from volcanic gas measurements obtained during 2003–2008 at Meakandake volcano, Hokkaido, Japan. Bull. Volcanol. 73, 409–421. http://dx.doi.org/10.1007/s00445-011-0463-2.

Stix, J., Williams-Jones, G., Hickson, C., 2008. The COSPEC cookbook: making SO_2 measurements at active volcanoes IAVCEI. Meth. Volcanol. 1.

Stoiber, R., Malinconico Jr., L., Williams, S., 1983. Use of the correlation spectrometer at volcanoes. In: Tazieff, H., Sabroux, J.C. (Eds.), Forecasting Volcanic Events. Elsevier, New York, pp. 425–444.

Tamburello, G., Kantzas, E., McGonigle, A., Aiuppa, A., Giudice, G., 2011a. UV camera measurements of fumarole field degassing (La Fossa crater, Vulcano Island). J. Volcanol. Geotherm. Res. 199, 47–52. http://dx.doi.org/10.1016/j.jvolgeores.2010.10.004.

Tamburello, G., McGonigle, A., Kantzas, E., Aiuppa, A., 2011b. Recent advances in ground-based ultraviolet remote sensing of volcanic SO_2 fluxes. Ann. Geophys. 54. http://dx.doi.org/10.4401/ag-5179.

Tamburello, G., Hansteen, T., Bredemeyer, S., Aiuppa, A., Tassi, F., 2014. Gas emissions from five volcanoes in northern Chile and implications for the volatiles budget of the Central Volcanic Zone. Geophys. Res. Lett. 41, 4961–4969. http://dx.doi.org/10.1002/2014GL060653.

Tassi, F., Aguilera, F., Vaselli, O., Darrah, T., Medina, E., 2011. Gas discharges from four remote volcanoes in northern Chile (Putana, Olca, Irruputuncu and Alitar): a geochemical survey. Ann. Geophys. 54.

Theys, N., Campion, R., Clarisse, L., Brenot, H., van Gent, J., Dils, B., Corradini, S., Merucci, L., Coheur, P.F., Van Roozendael, M., Hurtmans, D., Clerbaux, C., Tait, S., Ferrucci, F., 2013. Volcanic SO_2 fluxes derived from satellite data: a survey using OMI, GOME-2, IASI and MODIS. Atmos. Chem. Phys. 13, 5945–5968. http://dx.doi.org/10.5194/acp-13-5945-2013.

Vandaele, A., Hermans, C., Fally, S., 2009. Fourier transform measurements of SO2 absorption cross sections: II. Temperature dependence in the 29000–44000 cm-1 (227–345 nm) region. J. Quant. Spectrosc. Radiat. Transf. 110, 2115–2126.

Zelenski, M., Fischer, T., de Moor, J., Marty, B., Zimmermann, L., Ayalew, D., Nekrasov, A., Karandashev, V., 2013. Trace elements in the gas emissions from the Erta Ale volcano, Afar, Ethiopia. Chem. Geol. 357, 95–116. http://dx.doi.org/10.1016/j.chemgeo.2013.08.022.